Sorption of Rare Earth Metal Ions (La(III), Nd(III) and Er(III)) using Cellulose

Ahmed Galhoum, Asem Atia, Ahmad Tolba, Said Mohamady, Sally Mohammed, Eric Guibal

Sorption of Rare Earth Metal Ions (La(III), Nd(III) and Er(III)) Using Cellulose

Ahmed A. Galhoum[a,b*], Asem A. Atia[c], Ahmad A. Tolba[a], Said I. Mohamady[a], Sally S. Mohammed[a] and Eric Guibal[b*]

[a]*Nuclear Materials Authority, El-Maadi, Cairo, Egypt;* [b]*Centre des Matériaux des Mines d'Alès, Ecole des mines d'Alès, Alès, France;* [c]*Chemistry Department, Faculty of Science, Menoufia University, Shiben El-Kom, Egypt*

Abstract: ***Background:*** Rare earth elements, REEs, are used for many high-tech applications; the rare-faction of the resource requires developing methods for their recovery from low-grade sources and their recycling from waste materials. Sorption processes, including biosorbents, represent an interesting method for their recovery from dilute effluents.

Objective: This work investigates the sorption of 3 REEs using a cheap, renewable biosorbents: mi-crocrystalline cellulose (considered as a reference material for on-going research on chemically modified materials).

Methods: Sorption properties are studies considering the effect of pH, the uptake kinetics, sorption iso-therms, the thermodynamic parameters, the recycling of the material and reusing it for successive sorp-tion/desorption cycles.

Results: Metal sorption increases with pH, uptake kinetics are relatively fast with an equilibrium reached within 3-4 hours. The kinetic profiles are well fitted by the pseudo-second order rate equation. Maximum sorption capacity reaches 31-53 mg metal g^{-1}, and the Langmuir equation fits well sorption isotherms. The reaction is endothermic and spontaneous. Metal ions can be readily desorbed with 0.5 M HNO3 solutions and the sorbent can be recycled for at least 4 cycles of sorption/desorption with limited decrease in per-formance (less than 3 %). FTIR and XRD analyses contribute to the characterization of the material and the interpretation of sorption mechanism.

Conclusion: Microcrystalline cellulose has low sorption capacities for La(III), Nd(III), and Er(III); how-ever, this renewable resource with high effectiveness in terms of recycling and re-use is a promising sup-port for metal recovery.

Keywords: Cellulose, sorption isotherms, uptake kinetics, rare earth metal ions, metal desorption, sorbent recycling, sorption thermodynamics.

1. INTRODUCTION

The development of high-tech industries is requiring in-creasing amounts of precious and strategic metals such as platinum group metals or rare earth elements (REEs). The rarefaction of the resources, which is due to the limitation of primary mining resources and to geopolitical constraints for the access to target metals, has been the main incentive over the last decade for developing new processes for the recov-ery of valuable metals from the so-called urban mine, which is constituted of wastes of materials, such as WEEs [1, 2], infra-marginal ores and industrial wastes [3, 4]. Making a resource from a waste material recently became a credo for politics all over the world; and many incentive regulations have been promulgated for improving the recycling of stra-tegic metals [1, 5, 6]. REEs, including yttrium, scandium and the lanthanide series, are widely used for photo-electronic and metallurgical industries and in nuclear energy programs; as a consequence the demand for rare earth elements, and their alloys, is steadily increasing. The challenge for REE industry consists of the separation of REEs from base metals and the selective separation of individual REEs from mix-tures of REEs. Indeed, due to very similar electronic con-figurations their physicochemical properties are very close and numerous theoretical plates are required for separating these REEs [7].

Hydrometallurgy is offering a wide range of possibilities for recovering valuable metals from ores, waste materials and sub-products of industrial activities; leaching and

*Address correspondence to these authors at the Centre des Matériaux des Mines d'Alès, Ecole des mines d'Alès, 30319 Alès cedex, France; Tel: +33 (0)466782734; E-mails: eric.guibal@mines-ales.fr, Galhoum_nma@yahoo.com

bioleaching are typical methods that can be used for extracting metals from non-conventional metal sources [2-4]. The recovery of target metals from leachates may involve solvent extraction techniques [8-10]; however, this process is generally efficient for metal recovery from effluents with high metal-loading. For less-concentrated effluents, sorption process using ion-exchange, chelating resins [11-14] or solvent impregnated resins [15] are generally preferred. Biosorption has recently retained a great attention for metal binding from dilute solutions [16-20]. Biosorbents bear reactive groups similar to those found in synthetic resins; they are obtained from renewable resources including agriculture wastes, seaweeds, biomass derived from marine feedstock, etc. [19, 21]. They are generally less expensive than conventional resins. In addition, at the end of their life cycle their elimination is more environmentally friendly; the thermal degradation of synthetic resins may generate hazardous subproducts, especially toxic fumes, contrary to biosorbents. For example, alginate has been used for the recovery of lanthanum [20, 22] and other REEs [23, 24]. Chitosan-based sorbents have also retained a great attention for the last decade for the binding of REEs [16, 25-27], playing with the chemical versatility of the biopolymer and the possibility to graft specific functional groups. Despite its ready availability and wide range of applications, cellulose-based materials have received much less attention for the removal of REEs [28-30]. Cellulose, like chitosan or alginate, bears a huge number of hydroxyl groups that make this biopolymer a very hydrophilic sorbent;at least more hydrophilic than conventional synthetic materials.

The objective of this study consists of investigating the sorption properties of microcrystalline cellulose for the recovery of La(III), Nd(III) and Er(III). These three metal ions are representative of light and heavy REEs that are constituted by the cerium group (with elements: Sc, La, Ce, Pr, Nd, Pm, Sm, Eu, and Gd) and the yttrium (with elements: Y, Tb, Dy, Ho, Er, Tm, Yb, and Lu) [7]. Sometimes, Eu, Gd and Tb are ranked as an intermediary separate group. The classification of these REEs was initially associated to the solubility of their sodium double sulfate salts. The effect of pH is carried out before testing uptake kinetics and evaluating sorption isotherms at different temperatures for calculating thermodynamic parameters. The desorption of metal ions from loaded sorbent is tested and the sorption/desorption performances are compared over 4 cycles in order to evaluate the recycling of the material. This work is part of a wide research program that focuses on the sorption of uranium and rare earth metal ions using chemical derivatives of biopolymers, including cellulose and chitosan. Similar methodologies have been used in previously published papers [25, 31-33].

2. MATERIALS AND METHODS

2.1. Materials

Microcrystalline cellulose $(C_6H_{10}O_5)_n$, was purchased from Merck AG (Germany). The commercial average size of microcrystalline cellulose is reported close to 80 µm (Merck Avicel). Other common chemicals were supplied by Prolabo (France); they were used as received. La_2O_3, $NdCl_3$ and $ErCl_3.xH_2O$ were purchased from Alfa-Aesar (USA). These salts were burned off at 900 ^oC for 3 h; the residues were mineralized in concentrated hydrochloric acid under reflux. The solution was then diluted in demineralized water to prepare stock solutions at the concentration of 1 g metal L^{-1}. The "working" solutions were prepared at the appropriate concentration and target pH immediately prior to use by dilution of the stock solution with demineralized water to prevent possible micro-precipitation phenomena when solutions are stored for long time. The pH of the solutions was adjusted by addition of drops of aqueous NaOH and/or HCl solutions (0.05-1.0 mol L^{-1}).

2.2. Characterization of Materials

The FT-IR spectra were obtained after incorporation in KBr pellet using a JASCO-FT-IR-6600 spectrometer (Japan). X-ray diffraction (XRD) patterns were obtained at room temperature by X-Ray Diffractometry (RIGAKU, Japan), using the Cu K_α radiation in the range: 2θ = 10-80°. Thermogravimetric analysis was carried out using a TG/DTA 6300N, (Seiko Instruments Inc. (SII) Japan), under N_2/O_2 atmosphere at a constant heating rate of 10 °C min^{-1}. The morphology of the sorbents and their energy-dispersive X-ray analysis was investigated with FE-SEM Hitachi SU8020 microscope equipped with EDAX analyzer (Japan).

2.2. Adsorption and desorption experiments

Batch experiments were carried out by contact of 0.02 g of cellulose sorbent with 100 mL of aqueous solution (metal concentration, C_0: 100 mg L^{-1}) in a polypropylene flask under agitation (200 rpm) at 300 K for 3 hours. After equilibration and phase separation (filtration on 1.2 µm pore size membranes), the pH was recorded and the residual metal concentration in the aqueous phase was estimated by ICP-AES, inductively coupled plasma atomic emission spectrometry (Jobin Yvon Activa M, France), whilst the concentration of metal ions sorbed onto the functionalized cellulose was obtained by the mass balance equation, Eq. (1):

$$q_{eq} = (C_0 - C_{eq}) \times V/M \quad (1)$$

here q_{eq} is the amount of sorbed metal ions (mg metal g^{-1} sorbent), while C_0 and C_{eq} are the initial and equilibrium metal ion concentrations (mg metal L^{-1}) in the aqueous solution, respectively. V is the volume of the solution (0.1 L) and M is the mass of the sorbent (0.02 g).

Standard experimental conditions were set at T: 27 ± 1°C and pH: 5.00 ± 0.01; the contact time was fixed to 3 h. However, when relevant these parameters were varied for determining pH effect, sorption isotherm characteristics and uptake kinetics.

Isotherm studies were investigated by mixing 0.02 g of sorbent with 100 mL of metal RE(III) solution at different initial concentrations (i.e., 25, 50, 75, 100, 150 and 200 mg L^{-1}, at pH 5) and shaking for 3 h at 200 rpm. The experiments were performed in a thermostatic chamber, at different temperatures (293 ±1 K, 300 ±1 K, 313 ± 1 K and 323 ± 2 K).

Uptake kinetics were performed using a sorbent dosage of 0.2 g L^{-1} and a concentration of 100 mg metal L^{-1} at 300±1 K: samples were collected under agitation at standard times

and metal concentration was determined, after phase separation, by ICP-AES.

In addition, the recycling of the sorbents was tested by comparing the sorption capacity at different successive steps in a series of 4 sorption/desorption cycles: 0.02 g of sorbent was mixed with 100 mL of a REE solution (C_0: 100 mg metal L^{-1}) for 3 h at 27 °C in closed polyethylene flask. After phase separation the sorbent was recovered and the metal concentration in the supernatant was determined by ICP-AES: the mass balance equation was used for determining the sorption capacity and the sorption efficiency. After being washed with demineralized water, the metal-loaded sorbent was mixed with 50 mL of a 0.5 M HNO_3 solution for 60 min at 27 °C. The metal concentration in the supernatant was used for calculating by mass balance the desorption yield, at each step. The duplication or triplication of selected experiments showed that the standard deviation was systematically less than 6 %.

3. RESULTS AND DISCUSSION

3.1. Sorbent Characterization

FTIR spectrometry can be used for both the identification of functional groups at the surface of the sorbent and for the interpretation of sorption mechanisms while identifying the functional groups involved in metal binding groups: shift, appearance or disappearance of typical bands. The interpretation of changes is sometimes made difficult by the low sorption capacities and the low metal content in the sorbent Figure AM1 (see Additional Material Section) shows the FTIR spectra of both raw microcrystalline cellulose and metal-loaded sorbent. A large absorption band is observed around 3200-3300 cm^{-1}; this broad band is generally assigned to –OH stretching vibration. In raw microcrystalline cellulose the peak is detected at 3323.7 cm^{-1}, while the band is shifted to 3339.1 cm^{-1}, 3332.4 cm^{-1} and 3335.4 cm^{-1} after the sorption of La(III), Nd(III) and Er(III), respectively. This shift can be directly associated to the binding of metal ions, which affects the environment of OH groups. The peak at 2900 cm^{-1} (assigned to $–CH_2$ groups) is not affected by metal sorption. The band at 1425 cm^{-1} is assigned to intermolecular hydrogen bonds in the pyranose ring [34]. The bands in the region 960-1170 cm^{-1} are typically representative of pyranose ring skeletal (1160 cm^{-1}). The band at 1108 cm^{-1} is assigned to OH association [35]. The C-O stretching and C-O deformation vibrations (corresponding to C-OH in primary alcohol groups) are detected around 1060 cm^{-1}. The signals in the wavenumber range 700-400 cm^{-1} are usually assigned to C-C stretching while C-H bonds are identified in the range 700-900 cm^{-1} [35]. The comparison of the spectra before and after metal sorption shows very limited variations; this is probably due to the relatively low sorption (less than 50 mg metal g^{-1}) that makes difficult the detection of these differences.

Cadogan *et al.* [16] reported the sorption mechanism between chitosan and Eu(III) and identified the simultaneous contributions of C2-N and C6-OH groups on polymer chain and their “mirror” equivalent groups from adjacent polymer chain for binding Eu(III). Since other constituents of cellulose backbone are poorly reactive, a similar mechanism could be suggested in the case of cellulose with crossed interactions of C2-OH and C3-OH reactive groups of two adjacent chains according Scheme AM1 (see Additional Material Section).

Figure AM2 (see Additional Material Section) shows the XRD pattern of cellulose before and after the sorption of REE metal ions. The XRD pattern of microcrystalline cellulose shows 3 distinct planes at 2θ = 15, 16.4, 22.5 and 34.5 degrees. These peaks are characteristic of microcrystalline cellulose [36]. Actually, depending on the source raw cellulose can be constituted of two allomorphs,the so-called I_α and I_β forms. The broad peak at 2θ= 15/16.4 is associated to 100 I_α, 110 I_β and 010 I_β reflection planes, while the peak at 2θ = 22.5° is representative of 110 I_α and 200 I_β reflection planes. These peaks are common to the two cellulose forms: I_α, in algal and bacterial cellulose, and I_β in wood cellulose, cellulose forms [37]. However, peak at 2θ= 34.5° is typically representative of wood cellulose. The sorption of REE metal ions does not affect the XRD patterns: it is not possible to detect shift in the angle of diffraction of reference peaks and the full width at half maximum height (FWHM) is not significantly affected by the binding of metal ions. The low sorption capacities (see below) may explain the relatively limited effect of metal intercalation on the crystallinity of the biopolymer.

The thermal degradation of cellulose is easy compared to conventional resins both in terms of temperatures of degradation;close to T_{onset}: 250-270 °C and to T_{max}: 322 °C for the temperature at maximum weight-loss rate (Figure AM3, See Additional Material Section) and in terms of degradation products. Indeed, cellulose is degraded into CO_2 by combustion while for synthetic resins some hazardous volatile subproducts may be generated during combustion; r require proceeding to the incineration at very high temperature to prevent their emission [38]. This is an important criterion to take into account for the management of the life-cycle of the sorbent.

3.2. pH Effect on Metal Sorption

The effect of pH on the sorption of La(III), Nd(III) and Er(III) is reported in Fig. (**1**). The sorption capacity continuously increases with pH. This behavior can be directly correlated to the acid-base properties of cellulose. Cellulose is usually considered a weak acid [39-41]. Values of the pK_a in the range 3.7-4.2 have been reported depending on the ionic strength of the solution [39]; and even as high as 5.15 for 0.001 M NaCl solutions. This means that, depending on the pH of the solution, a partial release of protons from –OH groups can be expected. The pH of zero-charge is frequently reported lower than 2-3 [39, 42]. On the other hand, the proton may be exchanged with metal cations: this ion-exchange mechanism is enhanced at the higher pH due to the increased mobility/release of protons [42]. As the pH increases, the competition of protons from the solution with metal cations decreases and the sorption capacity increases. This proton exchange may be influenced by the ionic strength of the solution by competition effect (negative impact) and by the decrease in the pK_a of hydroxyl groups (positive impact). Zhu *et al.* [43] reported the increase in the sorption capacity for La(III) and Ce(III) using a composite made of acrylic acid, hydroxypropyl cellulose and attapulgite (crystalline

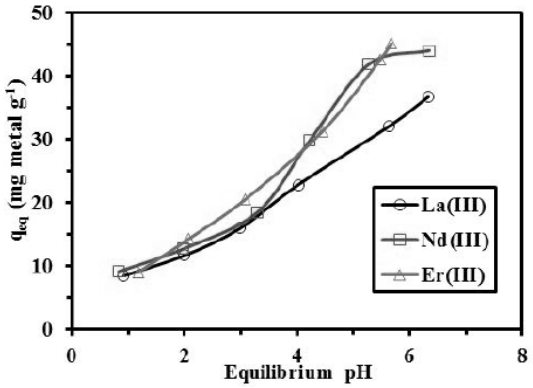

Fig. (1). Effect of equilibrium pH on the sorption of La(III) , Nd(III) and Er(III) ions using cellulose (C_0: 100 mg metal ion L^{-1}; T: 300 K; agitation time, t: 3 h; sorbent dosage, SD: 0.2 g L^{-1}).

hydrated magnesium silicate) when the pH increases: in this case they attribute metal cation sorption to a combination of chelation between hydroxyl, carboxylate groups and metals ions with electrostatic interaction between carboxylate groups and metal ions. The three REEs show very similar patterns regarding the impact of pH on metal sorption; playing with the pH is not expected to contribute to their selective separation in multi-component solutions.

The pH variation during the sorption is recorded in Figure AM4 (see Additional Material Section): the pH change was rather limited in the range pH 1-3 and tended to increase by 0.3-0.5 pH units above initial pH 3. Under selected metal concentrations the equilibrium pH was systematically below the limit pH value for metal precipitation, calculated by Medusa, [44]. However, at high pH values (higher than 6), and with higher metal concentrations as those used for establishing the sorption isotherms, some precipitation phenomena may occur and affects actual metal sorption. For this reason, the initial pH used for further studies was set at 5.

3.3. Uptake Kinetics

Figure **2** reports the kinetic profiles for the sorption of La(III), Nd(III) and Er(III) metal ions from pH 5 solutions (C_0: 100 mg REE L^{-1}; sorbent dosage, SD: 2 g L^{-1}). Two sections can be clearly identified (Fig. **2a**). Within the first 60 min of contact the uptake kinetics shows (for all REEs) a sharp increase in the sorption capacity; this section represents 81 to 86 % of the total sorption. This step corresponds to the fast sorption of REE metal ions at the surface of the sorbent, or within the first external layers of the particles. The sorption continues with a much slower step: the remaining 14 to 19 % of residual sorption occurs within the next 5 hours. This slow sorption is probably associated to the contribution of the mechanism of resistance to intraparticle diffusion. In order to gain a better understanding of controlling steps, which can include resistance to bulk diffusion, to film diffusion, to intraparticle diffusion, but also the proper reaction rate, several simple models have been used for fitting kinetic profiles.

The pseudo-first order reaction equation,PFORE, the so-called Lagergren equation, is linearized under the form [45]:

$$\text{Log}(q_{eq} - q(t)) = \log q_{eq} - (k_1/2.303)\, t \qquad (2)$$

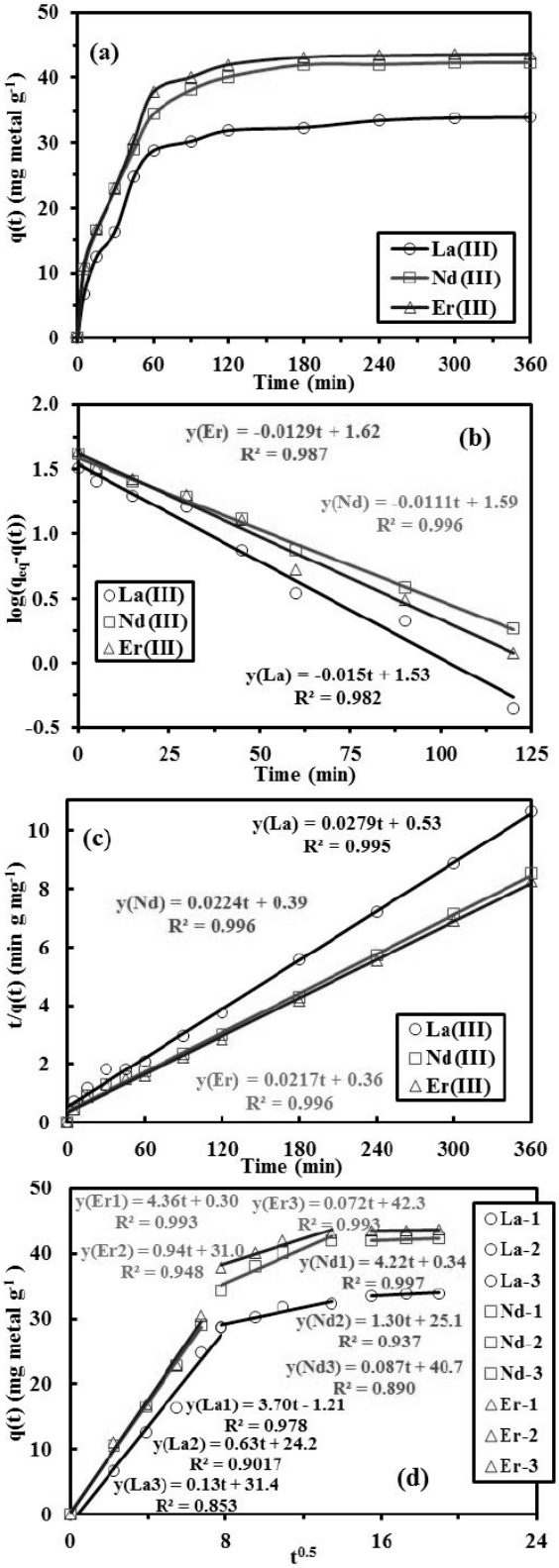

Fig. (2). RE(III) uptake kinetics using cellulose: (**a**) metal concentration in the sorbent *vs.* time, (**b**) PFORE plots, (**c**) PSORE plots. (**d**) sRIDE (pH_i: 5; C_0: 100 mg metal ion L^{-1}; T = 300 K; SD: 0.2 g L^{-1}).

The pseudo-second order rate equation (PSORE) is linearized under the form [45]:

$$t/q(t) = 1/k_2\, q_{eq}^{\,2} + (1/q_{eq})\, t \qquad (3)$$

Table 1. Uptake kinetics for La(III), Nd(III) and Er(II) sorption using cellulose – Parameters for the PFORE, the PSORE and the sRIDE models (C_0: 100 mg metal L^{-1}; pH_i: 5; sorbent dosage, SD: 0.2 g L^{-1}; T: 27 °C).

Metal ion		PFORE		
	$q_{eq,exp}$	$K_1 \times 10^{-2}$	$q_{eq,calc}$	R^2
La(III)	33.85	3.46	34.2	0.982
Nd(III)	42.30	2.56	38.7	0.996
Er(III)	43.65	2.97	41.6	0.987
Metal ion		**PSORE**		
	$q_{eq,exp}$	$K_2 \times 10^{-3}$	$q_{eq,calc}$	R^2
La(III)	33.85	1.46	35.84	0.995
Nd(III)	42.30	1.30	44.64	0.996
Er(III)	43.65	1.33	46.08	0.996
Metal ion		**sRIDE**		
		$K_{id,1}$	$K_{id,2}$	$K_{id,3}$
La(III)		3.70	0.6343	0.1308
Nd(III)		4.22	1.3041	0.0871
Er(III)		4.36	0.9396	0.072

Units: K_1: min^{-1}; K_2: g mg^{-1} min^{-1}; $K_{id,i}$: mg g^{-1} $min^{-0.5}$; q_{eq}: mg metal g^{-1}

where q_{eq} and q(t) (mg metal ion g^{-1}) are the sorption capacities at equilibrium and time t (min), respectively; k_1 (min^{-1}) and k_2 (g mg^{-1} min^{-1}) are the rate constant for PFORE and PSORE, respectively.

The modeling of experimental data with the PFORE and the PSORE is appearing in Figs. (**2b** and **2c**), respectively. The rate coefficients are reported in Table **1**. The comparison of the determination coefficients (R^2) shows that the PSORE generally fits better experimental data than the PFORE. In addition, the comparison of experimental values for the sorption capacity at equilibrium with the calculated model values shows a better correlation with the PSORE.

It is noteworthy that these equations that were initially developed for modeling chemical reaction in homogeneous systems are frequently applied to heterogeneous reactions, such as solid/liquid adsorption. This means that the parameters of the models should be considered as apparent rate coefficient that intrinsically integrates the contribution of the mechanisms of resistance to diffusion. The apparent rate coefficients were of the same order of magnitude for the 3 REEs (between 1.46×10^{-3} and 1.30×10^{-3} g mg^{-1} min^{-1}). This means that the sorption reaction rate cannot be used for separating the metals from multi-component solutions.

The resistance to intraparticle diffusion can be modeled using sophisticated models [46]. However, the simplified model developed by Weber and Morris [47] has also been frequently used for evaluating the contribution of resistance to intraparticle diffusion and for comparing the kinetic profiles with varying experimental conditions:

$$q(t) = k_{id.}\, t^{0.5} + C \qquad (4)$$

where q(t) (mg metal ion g^{-1}) is the amount of metal ions sorbed at time t (min), and $k_{id.}$ (mg g^{-1} $min^{-0.5}$) is the rate constant of intraparticle diffusion constant and C (mg metal g^{-1}) is usually associated to the thickness of the boundary layer [48]. The fact that the linear plots do not pass through the origin (i.e., $C \neq 0$) is generally attributed to the contribution of resistance to film diffusion and to the thickness of the boundary layer. Hameed *et al.* [49] commented that when the plot of q(t) *vs.* $t^{0.5}$ shows different linear sections the system is controlled by different successive steps of resistance to bulk diffusion (generally negligible), film diffusion and intraparticle diffusion, including intraparticle diffusion into pores of different sizes: macro-, meso- or micro-pores. Figure **2d** clearly shows the coexistence of different linear sections: the process is initially controlled by film diffusion before the mass transfer is influenced by intraparticle diffusion; the last section corresponds to pseudo equilibrium: sorbent swelling with additional sorption on the sorption sites located at the center of microcrystalline cellulose particles, or sorption into the micropores). The values of intraparticle diffusion rate constants: $k_{id,1}$, $k_{id,2}$ and $k_{id,3}$ are reported in Table **1**. Consistently with previous observations using the other models, the parameters were very close for the three metals. The first stage was slightly faster for Er(III) according the sequence: Er(III)>Nd(III)>La(III) while for the second stage followed a different trend (i.e., Nd(III)>Er(III)>La(III)); the last step, which corresponds tothe attainment of equilibrium was slightly faster for La(III). In any cases, the differences observed with the three REEs are not sufficient to count on uptake kinetics for effective separation of these metal ions.

Based on the kinetic modeling, sorption mechanism appears to be controlled by both intraparticle diffusion and metal binding by sorption on external reactive groups through surface sorption and within the first layers of the sorbent. The contribution of resistance to external diffusion cannot be completely neglected at the early stage of adsorption [50].

3.4. Sorption Isotherms and Thermodynamic Characteristics

Sorption tests were carried out at different metal concentrations and different temperatures in order to plot the sorption isotherms (sorption capacity, q_{eq} *vs.* C_{eq}, residual concentration) and determine the thermodynamic parameters. The sorption isotherm, at fixed temperature, represents the distribution, at equilibrium, of the solute (metal ion) between the solid and aqueous phases, changing initial metal concentration. Figure **3** shows the results obtained for La(III), Nd(III) and Er(III) sorption at pH 5 for temperatures in the range 20-50 °C. Regardless of the metal the sorption capacity increases with temperature: the sorption process is thus endothermic (see below for thermodynamic analysis).

As expected, regardless of the metal and the temperature, the sorption capacity continuously increases with metal concentration but tends to stabilize (saturation plateau) for residual concentrations in the range 150-200 mg metal L^{-1}. The appearance of the saturation plateau suggests that the sorption isotherm will be preferentially fitted by the Langmuir equation (Eq. 5) than by the Freundlich equation (Eq. 6) [51]:

Langmuir equation: $q_{eq} = (q_m \times K_L \times C_{eq})/(1+b \times C_{eq})$

$$q_{eq} = \frac{q_m \times b \times C_{eq}}{1+b \times C_{eq}} \quad (5)$$

Freundlich equation: $q_{eq} = k_F \times C_{eq}^{1/n}$ (6)

where q_{eq} and q_m are sorption capacities (mg metal g^{-1}) at residual concentration, C_{eq} (mg metal L^{-1}) and saturation of the monolayer, respectively. The coefficient K_L is the Langmuir constant (L mg^{-1}), and the coefficients K_F and n (heterogeneity factor) are the constants of the Freundlich equation. The parameters of the models are summarized in Table **2**: the determinations coefficients are systematically higher for Langmuir, compared to Freundlich; in addition, the maximum sorption capacity, both experimental and calculated from the saturation of the monolayer (i.e., q_m) increases with temperature. Figure AM5 (see Additional Material Section) reports the linearization of experimental sorption isotherms with the Langmuir equation.

Two other models are frequently tested for modeling sorption isotherms: (a) the Dubinin-Radushkevich (D-R) model (Eq. 8), which can be used for calculating the mean free sorption energy E_{DR} (kJ mol^{-1}), and (b) the Temkin model (Eq. 9) [51]:

Dubinin-Raduskevich equation:

$$\ln q_{eq} = \ln q_{DR} - K_{DR}\varepsilon^2 \quad (8a)$$

with: $\varepsilon = RT \ln(1 + 1/C_{eq})$, (8b)

q_{DR} is the theoretical saturation capacity, while ε is the Polanyi potential. K_{DR} is the constant of the DR model associated to the mean free sorption energy per molecule of target sorbent ($E_{DR}=(2\ K_{DR})^{-1/2}$).

Table 2. Sorption isotherms for La(III), Nd(III) and Er(II) recovery using cellulose – Parameters for the Langmuir, and Freundlich models (pH_i: 5).

Metal ion	Temp. (K)	$q_{m,exp.}$ (mg g^{-1})	Langmuir			Freundlich		
			$q_{m,calc}$ (mg g^{-1})	$K_L \times 10^3$ (L mg^{-1})	R^2	1/n	K_F	R^2
La(III)	293	31.1	33.1	81.1	0.999	0.099	14.8	0.981
	300	33.7	35.9	82.9	0.998	0.101	16.1	0.974
	313	35.8	38.0	89.8	0.999	0.104	17.2	0.964
	323	38.4	40.7	90.5	0.999	0.104	18.6	0.954
Nd(III)	293	40.3	42.7	98.2	0.991	0.224	13.7	0.957
	300	44.6	47.2	100.5	0.996	0.283	21.9	0.980
	313	48.4	51.2	102.5	0.997	0.272	23.8	0.980
	323	51.1	54.1	103.2	0.998	0.244	25.4	0.980
Er(III)	293	41.5	44.0	96.4	0.999	0.143	20.3	0.984
	300	45.4	48.0	99.4	0.999	0.142	22.3	0.983
	313	49.2	52.0	101.1	0.999	0.141	24.3	0.984
	323	52.4	55.3	105.2	0.999	0.141	26.0	0.981

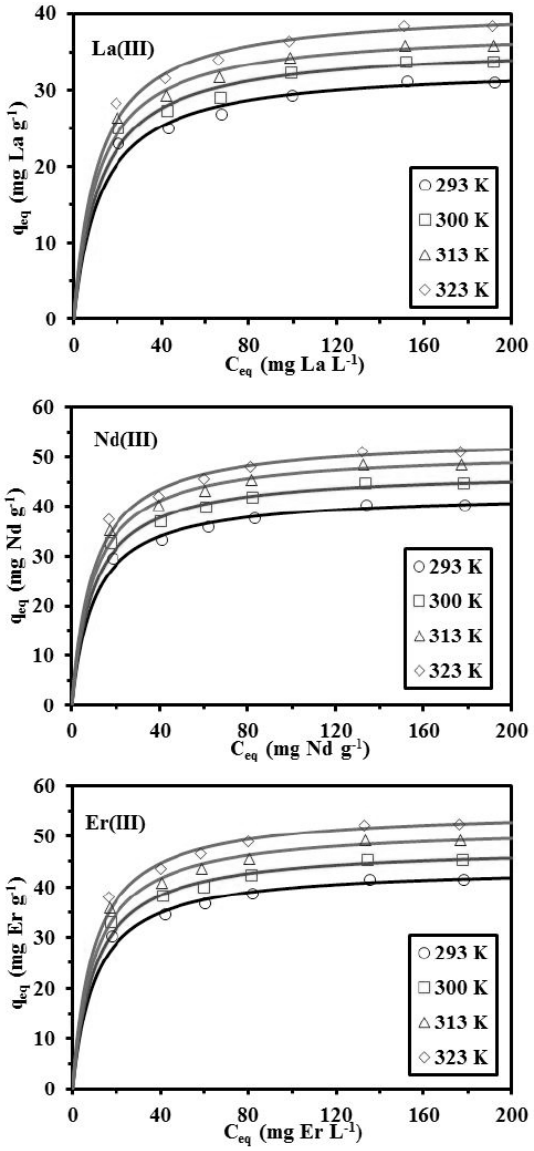

Fig. (3). Sorption isotherms of La(III) , Nd(III) and Er(III) ions at different temperatures using Cellulose (pH_i: 5; t: 3 h; SD: 0.2 g L^{-1}).

Temkin equation:

$$q_{eq} = B_T \ln C_{eq} + B_T \ln A_T \quad (9)$$

where A_T is the equilibrium-binding constant that corresponds to the maximum binding energy; this reflects the initial sorption heat. B_T is the constant related to heterogeneity of the sorbent surface, T is the absolute temperature (K), and R is the ideal gas constant (8.314 J mol^{-1} K^{-1}). The constants can be obtained from the slope and intercept of the straight line plot of q_{eq} versus ln C_{eq} (Figure AM6, see Additional Material Section).

The parameters of the DR and Temkin models are reported in Table **3**, while Figure AM3 (see Additional Material Section) shows the linearization of DR model for experimental data. As expected the maximum sorption capacity for DR model increases with the temperature, regardless of the REE; the mean free sorption energy (E_{DR}) also increases with temperature from 6.2 to 7.4 kJ mol^{-1}. Regardless of the metal and the temperature, the value of E_{DR} is systematically below the value of 8 kJ mol^{-1}, which is generally considered as the limit value for making the difference between physical adsorption (< 8 kJ mol^{-1}) and chemical adsorption (> 8 kJ mol^{-1}). Regarding the impact of temperature on EDR, it is noteworthy that Er(III) is the REE that was less influenced by temperature ($\Delta E_{DR/T}$= 0.2), contrary to La(III) ($\Delta E_{DR/T}$= 0.7) and Nd(III) ($\Delta E_{DR/T}$= 0.9).

In the Temkin model, the value of A_T is associated to the initial sorption heat of the sorbent for target metal, which iscorrelated to the affinity of the sorbent for the metal. The sorption heat increases with temperature, as well as the BT , which is associated to the heterogeneity of sorbent surface. However, these differences are relatively small. The A_T values for Nd(III) and Er(III) are of the same order of magnitude, in the range 20-25 L mg^{-1}, and higher than the values obtained for La(III), in the range 16-19 L mg^{-1}: microcrystalline cellulose has higher affinity for Er(III) and Nd(III) (almost equivalent) than for La(III).

The experimental data obtained at different temperatures were used for calculating the thermodynamics parameters: standard Gibbs free energy change (ΔG°), enthalpy change (ΔH°) and entropy change (ΔS°) were derived from Van't Hoff equation (Eq. (10) and (11).

$$\ln K_L = (-\Delta H°/R)\ 1/T + \Delta S°/R \quad (10)$$

$$\Delta G° = \Delta H° - T\Delta S° \quad (11)$$

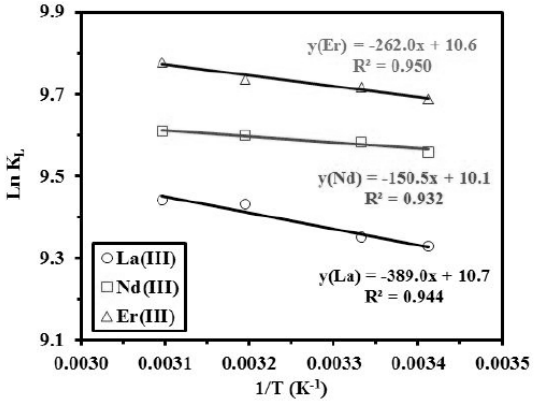

Fig. (4). Van't Hoff plots of ln K_L against 1/T, (K^{-1}) for RE(III) sorption using cellulose.

The values of enthalpy change (ΔH°) and entropy change (ΔS°) were obtained by plotting ln b against 1/T (Fig. **4**). The values of ΔH°, ΔS° and ΔG° are reported on Table **4**. The positive value of enthalpy change confirms that the sorption of the three REEs on microcrystalline cellulose is endothermic. This enthalpy change is associated to the combination of two enthalpy changes for (a) the dehydration or breaking of ion-water and water-water bonds of hydrated metal ions, and (b) the proper complexation reaction between the reactive groups of the sorbent and metal ions [52]. The negative value of free energy and the decrease in the value of ΔG^o with increase in temperature shows that the reaction is enhanced at high temperature. The positive value of ΔS^o may be related to the liberation of water of hydration during the sorption process causing the increase in the randomness of the system. The data showed that $|\Delta H°| < |T\Delta S°|$. This

Table 3. Sorption isotherms for La(III), Nd(III) and Er(II) recovery using cellulose - Parameters for the Dubinin-Raduskevich, and Temkin models (pH_i: 5).

Metal ion	Temp. (K)	D-R			Temkin		
		q_{DR} (mg g^{-1})	E_{DR} (kJ mol^{-1})	R^2	A_T (L mg^{-1})	B_T (J mol^{-1})	R^2
La(III)	293	31.0	6.16	0.898	16.0	3.91	0.975
	300	33.7	6.35	0.888	16.4	4.24	0.963
	313	36.1	6.59	0.939	17.9	4.48	0.982
	323	37.5	6.84	0.948	19.1	4.76	0.988
Nd(III)	293	40.7	6.46	0.956	20.8	5.01	0.984
	300	45.1	6.65	0.990	21.5	5.52	0.985
	313	48.9	7.00	0.962	22.2	5.97	0.985
	323	51.5	7.37	0.946	24.7	6.22	0.983
Er(III)	293	42.0	6.87	0.956	20.6	5.14	0.987
	300	45.9	6.93	0.962	22.7	5.56	0.988
	313	49.7	7.00	0.957	23.7	6.00	0.987
	323	53.0	7.04	0.962	25.1	6.36	0.986

Table 4. Thermodynamic parameters of La(III), Nd(III) and Er(III) ions sorption using Cellulose.

Metal Ion	Temp., K	ΔH^0 kJ mol^{-1}	ΔS^0 J mol^{-1} K^{-1}	ΔG^0 kJ mol^{-1}	$T\Delta S^0$ kJ mol^{-1}	R^2
La(III)	293	32.3	88.6	-22.7	26.0	0.944
	300			-23.3	26.6	
	313			-24.5	27.7	
	323			-25.4	28.6	
Nd(III)	293	12.5	83.8	-23.3	24.6	0.932
	300			-23.9	25.1	
	313			-25.0	26.2	
	323			-25.8	27.1	
Er(III)	293	21.7	88.0	-23.6	24.6	0.950
	300			-24.2	25.8	
	313			-25.4	27.5	
	323			-26.2	28.4	

means that the sorption process is dominated by entropic rather than enthalpic changes [25].

3.5. Comparison of Sorption Properties with Literature

The sorption properties for selected REEs by microcrystalline cellulose are compared to relevant values reported in the literature (Table **5**) [25, 27, 32, 53-61]. This material is supposed to constitute the reference material for on-going studies on the grafting of specific reactive groups, such as thiourea, poly(carboxyl)/pol(amine) groups. Obviously the maximum sorption capacities of this simple material are relatively low compared to the most efficient sorbents such as activated carbon derived from rice husk for La(III) (175 mg La g^{-1} *vs.* 38 mg La g^{-1}), phosphorus-functionalized adsorbent for Nd(III)

Table 5. Comparison of sorption capacity for La(III), Nd(III) and Er(III) ions with various sorbents.

Metal Ion	Sorbent	pH_i	T (K)	q_{max} (mg g^{-1})	Reference
La(III)	Magnetic aminated-chitosan nanobased particles	5	320	50.2	[25]
	Activated carbon derived from rice husk	3.5	293	175.4	[53]
	Tannic acid/multi-walled carbon nanotubes	4	293	9.8	[54]
	SiO_2-TiO_2-NCs nanocomposite	5	298	65.6	[55]
	Polydopamine/nanofibrous mats	4.5	298	59.4	[56]
	Cysteine-chitosan magnetic nanobased particles	5	320	21.3	[32]
	Cellulose	5	323	38.4	This work
Nd(III)	Magnetic aminated-chitosan nanobased particles	5	320	51.5	[25]
	EDTA and DTPA/chitosan	3-6	298	77.0	[27]
	Ion-imprinted particles	7.5	(a)	33.0	[57]
	Phosphorus-functionalized sorbent	6	(a)	160.0	[58]
	Phosphonic acid/silica microspheres	2-8	(a)	45.0	[59]
	Cysteine-functionalized chitosan magnetic nanobased particles	5	325	35.0	[32]
	Cellulose	5	323	51.1	This work
Er(III)	D113-III resin	6	298	250.0	[60]
	Activated carbon derived from rice husk	3.5-5	303	250.0	[53]
	Activated charcoal	4	323	225.6	[61]
	Cellulose	5	323	52.4	This work

(160 mg Nd g^{-1} *vs.* 51 mg Nd g^{-1}), or D1113-III resin for Er(III) (250 mg Er g^{-1} *vs.* 53 mg Er g^{-1}). However; the values of the maximum sorption capacities are roughly of the same order of magnitude than most of the conventional materials found in the literature. These sorption performances will be considered as base values for the chemical modification of the raw material (on-going research).

3.6. Metal Desorption and Sorbent Recycling

The evaluation of the efficiency of a sorbent and its ability to be applied at large scale should take into account its capacity to be desorbed and re-used. Indeed, metal desorption may contribute to improve the competitiveness of the sorbent, its selective separation properties or its enrichment factor. In order to evaluate these properties, 4 successive sorption/desorption cycles were operated and the sorption and desorption efficiencies were compared under identical experimental conditions (Table **6**).

REE desorption from metal-loaded cellulose is efficiently operated using 0.5 M HCl solutions: the efficiency of desorption slightly decreases with the number of cycles but even after 4 cycles the desorption yield exceeds 92 % : the loss is limited to 2 % between the first and last cycle). In addition, the comparison of the sorption levels, under selected experimental conditions, remained higher than 91 %: the decrease in sorption efficiency does not exceed 2-3 %.

The sorption and desorption properties are remarkably stable and confirm that microcrystalline cellulose can be re-used for the sorption of La(III), Nd(III) and Er(III) for a minimum of 4 sorption/desorption cycles. Alternating sorption and desorption steps may induce a degradation of the material by hydrolysis of the biopolymer; however, the relative stability of the sorption/desorption performance means that this degradation remains negligible at least in terms of metal binding for 4 cycles: extending the re-use of the material over 4 cycles would probably contribute to increase the degradation of the sorbent and limits its sorption performances.

CONCLUSIONS AND PERSPECTIVES

This study shows that microcrystalline cellulose has the potential to bind rare-earth metal ions such as La(III),

Table 6. Sorption performance (sorption and desorption efficiencies, %) for 4 successive sorption/desorption cycles for the recovery of La(III), Nd(III) and Er(III) ions using cellulose.

Cycle number	La(III)		Nd(III)		Er(III)	
	S (%)	D (%)	S (%)	D (%)	S (%)	D (%)
Cycle I	93.0	93.3	94.0	94.1	94.4	94.9
Cycle II	92.1	92.6	93.2	93.8	94.0	94.3
Cycle III	91.5	92.3	93.0	93.4	93.0	93.5
Cycle IV	91.3	91.8	91.8	92.1	92.2	93.0

Nd(III), which belong toCerium group of REEs (i.e., light rare-earth elements) and Er(III), which is part of Yttrium group of REEs (i.e., heavy rare-earth elements) at pH close to 5. Sorption levels are relatively low, in the range 31-53 mg REE g^{-1}, compared to some values collected in literature; however, this renewable resource is relatively cheap making the material interesting for further investigations. This material is relatively cheap (cost range: 1-5 USD/kg close to the quotes of SiO_2, TiO_2, and little higher than activated charcoal: 1-2 USD/kg)), it is readily regenerated and recycled and can be environmentally-friendly eliminated at the end of it life cycle. In addition, these values are considered as reference level for an on-going research on chemical modification of cellulose-based sorbents, obtained by grafting amino groups, carboxylic groups or sulfur groups, for enhanced sorption of rare-earth metal ions. The readily desorption of bound metal ions with 0.5 M HCl solution, and successful re-use of the sorbent, is also an important advantage of this simple material. Sorption capacities increase with temperature: the sorption process is endothermic, with enthalpy changes in the range 12.5-32.3 kJ mol^{-1} (depending on the metal) and is controlled by enthalpic rather than entropic change: entropy varies between 84 and 89 J mol^{-1}, while free Gibbs energy varies between 22 and 27 kJ mol^{-1}. The kinetic profiles are controlled by the resistance to intraparticle diffusion (mechanisms of resistance to intraparticle diffusion through pores of different sizes); however, the pseudo-second order rate equation fits well uptake kinetics.

It is noteworthy that the sorption performances, both in terms of equilibrium and kinetics, are hardly affected by the type of metal (i.e., light and/or heavy REEs). Though sorption was not investigated in multi-component solutions the results suggest that the separation of the REEs cannot be successfully achieved with microcrystalline cellulose. However the availability of this cheap re-usable renewable resource may be interesting for the broad recovery of REEs.

CONFLICT OF INTEREST

The authors confirm that this article content has no conflict of interest.

ACKNOWLEDGEMENTS

This work was supported by the International Atomic Energy Agency for financial support (IAEA for TC project number (Oracle Project No.: 1060242) and Fellowship Code Number: C6/EGY/15019). Authors acknowledge Mr. Thierry Vincent (Ecole des mines d'Alès, France) for technical support. Special dedication to the memory of Prof. Dr. Ahmed Donia.

ADDITIONAL MATERIAL

Additional material available.

REFERENCES

[1] Sun Z, Xiao Y, Agterhuis H, Sietsma J, Yang Y, Recycling of metals from urban mines a strategic evaluation. J Cleaner Prod 2016; 112: 2977-87.

[2] Tunsu C, Petranikova M, Gergoric M, *et al.* Reclaiming rare earth elements from end-of-life products: A review of the perspectives for urban mining using hydrometallurgical unit operations, Hydrometallurgy 2015; 156: 239-58.

[3] Borra CR, Pontikes Y, Binnemans K, Van Gerven T. Leaching of rare earths from bauxite residue (red mud), Miner Eng 2015; 76: 20-7.

[4] Sinha S, Meshram P, Pandey BD, *et al.* Metallurgical processes for the recovery and recycling of lanthanum from various resources-A review, Hydrometallurgy 2016; 160: 47-59.

[5] Gutierrez-Gutierrez SC, Coulon F, Jiang Y, Wagland ST. Rare earth elements and critical metal content of extracted landfilled material and potential recovery opportunities. Waste Manage 2015; 42: 128-36.

[6] Liu Z, Li H. Metallurgical process for valuable elements recovery from red mud-A review. Hydrometallurgy 2015; 155: 29-43.

[7] Cotton S, Lanthanide and Actinide Chemistry, Chichester, UK, John Wiley & Sons, Ltd., 2006, 263.

[8] Abreu RD, Morais CA. Study on separation of heavy rare earth elements by solvent extraction with organophosphorus acids and amine reagents. Miner Eng 2014; 61: 82-7.

[9] Vander HT, Binnemans K. Highly efficient separation of rare earths from nickel and cobalt by solvent extraction with the ionic liquid trihexyl(tetradecyl) phosphonium nitrate: A process relevant to the recycling of rare earths from permanent magnets and nickel metal hydride batteries. Green Chem 2014; 16(3): 1594-606.

[10] Xia Y, Xiao L, Tian J, Li Z, Zeng L. Recovery of rare earths from acid leach solutions of spent nickel-metal hydride batteries using solvent extraction. J Rare Earths 2015; 33(12): 1348-54.

[11] Hubicka H, Kołodyńska D. Studies on application of polyacrylate anion-exchangers in sorption and separation of iminodiacetate rare earth element(III) complexes. Hydrometallurgy 2001; 62(2): 107-13.

[12] Kim J-G. Separation of heavy rare earth elements with extraction chromatography. Curr Nanosci 2014; 10(1): 11-5.

[13] Xiong C, Liu X, Yao C. Effect of pH on sorption for RE(III) and sorption behaviors of Sm(III) by D152 resin. J Rare Earths 2008; 26(6): 851-6.

[14] Xiong C, Rao C. Use of gel-type weak acid resin for the adsorption of La(III) from aqueous solution. Indian J Chem Technol 2012; 19(6): 392-8.

[15] Zhang L, Wu D, Zhu B, Yang Y, Wang L. Adsorption and selective separation of neodymium with magnetic alginate microcap-

sules containing the extractant 2-ethylhexyl phosphonic acid mono-2-ethylhexyl ester. J Chem Eng Data 2011; 56(5): 2280-9.
[16] Cadogan EI, Lee C-H, Popuri SR, Lin H-Y. Efficiencies of chitosan nanoparticles and crab shell particles in europium uptake from aqueous solutions through biosorption: Synthesis and characterization, Int. Biodeterior. Biodegrad 2014; 95: 232-40.
[17] Das N, Das D. Recovery of rare earth metals through biosorption: An overview. J Rare Earths 2013; 31(10): 933-43.
[18] Koto Y, Kano N, Wang Y, Sakamoto N, Imaizumi H. Biosorption of lanthanides from aqueous solutions using pretreated *Buccinum tenuissimum* shell biomass. Bioinorg Chem Appl 2010; doi:10.1155/2010/804854.
[19] Oliveira RC, Guibal E, Garcia O, Jr., *et al*. Biosorption and desorption of lanthanum(III) and neodymium(III) in fixed-bed columns with *Sargassum sp*.: Perspectives for separation of rare earth metals. Biotechnol Progr 2012; 28(3): 715-22.
[20] Song D, Park S-J, Kang HW, Park SB, Han J-I, Recovery of lithium(I), strontium(II), and lanthanum(III) using Ca-alginate beads. J Chem Eng Data 2013; 58(9): 2455-64.
[21] Oliveira RC, Jouannin C, Guibal E, Garcia O Jr., Samarium(III) and praseodymium(III) biosorption on *Sargassum sp*.: Batch study. Proc Biochem 2011; 46(3): 736-44.
[22] Wu D, Zhang L, Wang L, Zhu B, Fan L. Adsorption of lanthanum by magnetic alginate-chitosan gel beads. J Chem Technol Biotechnol 2011; 86(3): 345-52.
[23] Wang F, Zhao J, Wei X, *et al*. Adsorption of rare earths (III) by calcium alginate-poly glutamic acid hybrid gels. J Chem Technol Biotechnol 2014; 89(7): 969-77.
[24] Xu S, Wang Z, Gao Y, Zhang S, Wu K. Adsorption of rare earths(III) using an efficient sodium alginate hydrogel cross-linked with poly-gamma-glutamate. Plos One 2015; 10(5) : e0124826.
[25] Galhoum AA, Mahfouz MG, Abdel-Rehem ST, *et al*. Diethylenetriamine-functionalized chitosan magnetic nano-based particles for the sorption of rare earth metal ions Nd(III), Dy(III) and Yb(III), Cellulose 2015; 22(4): 2589-605.
[26] Haldorai Y, Rengaraj A, Ryu T, *et al*. Response surface methodology for the optimization of lanthanum removal from an aqueous solution using a Fe_3O_4/chitosan nanocomposite. Mater Sci Eng B 2015; 195: 20-9.
[27] Roosen J, Binnemans K. Adsorption and chromatographic separation of rare earths with EDTA- and DTPA-functionalized chitosan biopolymers. J Mater Chem A 2014; 2(5): 1530-40.
[28] Oshima T, Kondo K, Ohto K, Inoue K, Baba Y. Preparation of phosphorylated bacterial cellulose as an adsorbent for metal ions. React Funct Polym 2008; 68(1): 376-83.
[29] Takeda Y, Ishida K. Thin-layer chromatography of rare earth elements in carboxymethyl cellulose-aqueous sodium chloride systems and the specific separation of yttrium, Bunseki Kagaku 2004; 53(7): 729-34.
[30] Takeda Y, Ishida K. Thin-layer chromatography of rare earths in a carboxymethyl cellulose-aqueous sodium nitrate system, and the separation of yttrium, Bunseki Kagaku 2004; 53(11): 1325-8.
[31] Galhoum AA, Atia AA, Mahfouz MG, *et al*. Dy(III) recovery from dilute solutions using magnetic-chitosan nano-based particles grafted with amino acids. J Mater Sci 2015; 50(7): 2832-48.
[32] Galhoum AA, Mafhouz MG, Abdel-Rehem ST, *et al*. Cysteine-functionalized chitosan magnetic nano-based particles for the recovery of light and heavy rare earth metals: Uptake kinetics and sorption isotherms. Nanomaterials 2015; 5(1): 154-79.
[33] Galhoum AA, Mahfouz MG, Atia AA, *et al*. Alanine and serine functionalized magnetic nano-based particles for sorption of Nd(III) and Yb(III). Adv Environ Res 2016; 5(1): 1-18.
[34] Haafiz MKM, Eichhorn SJ, Hassan A, Jawaid M. Isolation and characterization of microcrystalline cellulose from oil palm biomass residue. Carbohydr Polym 2013; 93(2): 628-34.
[35] Yang HP, Yan R, Chen HP, Lee DH, Zheng CG. Characteristics of hemicellulose, cellulose and lignin pyrolysis. Fuel 2007; 86(12-13): 1781-8.
[36] de Oliveira RL, Barud HdS, de Assuncao RMN, *et al*. Synthesis and characterization of microcrystalline cellulose produced from bacterial cellulose. J Therm Anal Calorim 2011; 106(3): 703-9.
[37] Mohite BV, Patil SV. Physical, structural, mechanical and thermal characterization of bacterial cellulose by G. hansenii NCIM 2529. Carbohydr Polym 2014; 106: 132-41.
[38] Dubois MA, Dozol JF, Nicotra C, Serose J, Massiani C. Pyrolysis and incineration of cationic and anionic ion-exchange resins - identification of volatile degradation compounds. J Anal Appl Pyrolysis 1995; 31: 129-40.
[39] Herrington TM, Midmore BR. Adsorption of ions at the cellulose aqueous-electrolyte interface. 1. Charge pH isotherms. J Chem Soc Faraday Trans 1 F 1984; 80: 1525-37.
[40] Herrington TM, Midmore BR. Adsorption of ions at the cellulose aqueous-electrolyte interface 3. Calculation of the potential at the surface of cellulose fibers. J Chem Soc Faraday Trans 1984; 80: 1553-66.
[41] Hubbe MA, Rojas OJ. Colloidal stability and aggregation of lignocellulosic materials in aqueous suspension: A review. Bioresources 2008; 3(4): 1419-91.
[42] Hubbe MA, Hasan SH, Ducoste JJ. Cellulosic substrates for removal of pollutants from aqueous systems: A review. 1. Metals, Bioresources 2011; 6(2): 2161-U2914.
[43] Zhu Y, Zheng Y, Wang A. A simple approach to fabricate granular adsorbent for adsorption of rare elements. Int J Biol Macromol 2015; 72: 410-20.
[44] Puigdomenech I. MEDUSA (Make equilibrium diagrams using sophisticated algorithms), in, Royal Institute of Technology, Stockholm, Sweden, 2010.
[45] Ho YS, McKay G, Pseudo-second order model for sorption processes. Proc Biochem 1999; 34(5): 451-65.
[46] Tien C. Adsorption Calculations and Modeling, Newton, MA, Butterworth-Heinemann, 1994, 243.
[47] Weber WJ, Morris JC. Kinetics of adsorption on carbon from solutions. J Sanitary Eng Div ASCE 1963; 89: 31-60.
[48] Cheung WH, Szeto YS, McKay G. Intraparticle diffusion processes during acid dye adsorption onto chitosan. Bioresour Technol 2007; 98(15): 2897-904.
[49] Hameed BH, Tan IAW, Ahmad AL. Adsorption isotherm, kinetic modeling and mechanism of 2,4,6-trichlorophenol on coconut husk-based activated carbon, Chem Eng J 2008; 144(2): 235-44.
[50] McKay G, Otterburn MS, Aga JA. Intraparticle diffusion process occuring during adsorption of dyestuffs. Water Air Soil Pollut 1987; 36(3-4): 381-90.
[51] Foo KY, Hameed BH. Insights into the modeling of adsorption isotherm systems. Chem Eng J 2010; 156(1): 2-10.
[52] Mahfouz MG, Killa HM, Sheta ME, Moustafa AH, Tolba AA. Synthesis, characterization, and application of polystyrene adsorbents containing tri-n-butylphosphate for solid-phase extraction of uranium (VI) from aqueous nitrate solutions. J Radioanal Nucl Chem 2014; 301(3): 739-49.
[53] Awwad NS, Gad HMH, Ahmad MI, Aly HF. Sorption of lanthanum and erbium from aqueous solution by activated carbon prepared from rice husk. Colloids Surf B 2010; 81(2): 593-9.
[54] Tong S, Zhao S, Zhou W, Li R, Jia Q. Modification of multi-walled carbon nanotubes with tannic acid for the adsorption of La, Tb and Lu ions. Microchim Acta 2011; 174(3-4): 257-64.
[55] Rahman MM, Khan SB, Marwani HM, Asiri AM. SnO_2-TiO_2 nanocomposites as new adsorbent for efficient removal of La(III) ions from aqueous solutions. J Taiwan Inst Chem Eng 2014; 45(4): 1964-74.
[56] Hong G, Shen L, Wang M, *et al*. Nanofibrous polydopamine complex membranes for adsorption of lanthanum (III) ions. Chem Eng J 2014; 244: 307-16.
[57] Krishna PG, Gladis JM, Rao TP, Naidu GR. Selective recognition of neodymium(III) using ion imprinted polymer particles. J Mol Recognit 2005; 18(1): 109-16.
[58] Park H-J, Tavlarides LL. Adsorption of neodymium(III) from aqueous solutions using a phosphorus functionalized adsorbent. Ind Eng Chem Res 2010; 49(24): 12567-75.
[59] Melnyk IV, Goncharyk VP, Kozhara LI, *et al*. Sorption properties of porous spray-dried microspheres functionalized by phosphonic acid groups. Microporous Mesoporous Mater 2012; 153: 171-77.
[60] Xiong C, Meng Y, Yao C, Shen C. Adsorption of erbium(III) on D113-III resin from aqueous solutions: Batch and column studies. J Rare Earths 2009; 27(6): 923-31.
[61] Qadeer R. Adsorption of erbium ions on activated charcoal from aqueous solutions. Colloids Surf A 2005; 254(1-3): 17-21.